Functional renormalization group study of the chiral phase transition with repulsive interactions

Defu Hou

Institute of particle Physics, Central China Normal University, Wuhan

Functional renormalization group study of the quark-meson model with ω meson, Zhang, Hou, Kojo, Qin, Phys.Rev.D 96 (2017) 11, 114029

Functional renormalization group study of the quark-meson model with omega and rho vector mesons, Osman, Hou, Wang, Zhang, Eur. Phys. J. C 85, 804 (2025)

Functional renormalization group study of rho condensate at a finite isospin chemical potential in the quark meson model, Osman, Hou, Wang, Zhang, arXiv: 2508.02745

Outline

Motivation and Background

Chiral Phase Structure with vector mesons

Isospin–Asymmetric QCD at Finite μ_I

Summary

Table of Contents

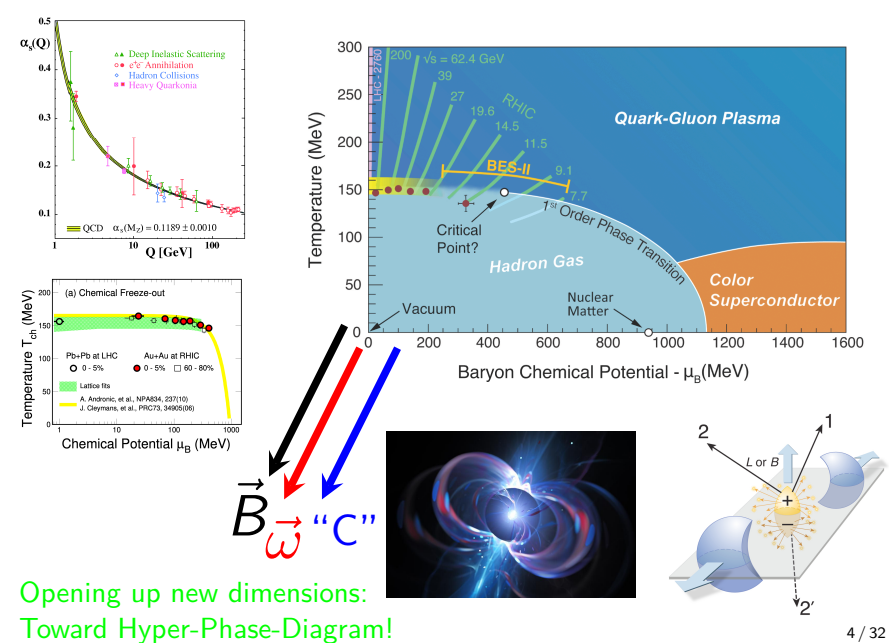
Motivation and Background

Chiral Phase Structure with vector mesons

Isospin–Asymmetric QCD at Finite μ_{I}

Summary

QCD Phase Diagram



Motivation and Background

- ▶ Finite- μ_I as a clean laboratory: the μ_I direction is sign-problem free, so models can be benchmarked directly against lattice constraints. An RG-invariant mean-field framework reproduces lattice phase boundaries and the EoS at small-intermediate μ_I . [Brandt *et al.*, Phys. Rev. D (2025)]
- ▶ Onset and crossover: the threshold for pion condensation is $\mu_I = m_\pi$; with increasing μ_I the soft mode exhibits a continuous BEC→BCS crossover. [He–Jin–Zhuang, Phys. Rev. D **71** (2005); Wang & Zhuang, Phys. Rev. D **96**, 014006 (2017)]
- ▶ Stiff matter at high μ_l : in a unified treatment the speed of sound c_s^2 can exceed the conformal value 1/3 in pion-condensed/2SC-like regimes, consistent with lattice/ χ PT trends. [Fukushima, Phys. Rev. D 111, 094006 (2025)]

Motivation and Background: Methods / Anchors

- ▶ **QCD**-assisted **fRG**: integrates quantum/thermal/density fluctuations and yields a phase structure and CEP region compatible with state-of-the-art lattice curvature near $\mu_B \simeq 0$. [Fu, Pawlowski & Rennecke, arXiv:1909.02991]
- ▶ **High-order fluctuation diagnostics:** fRG results for baryon-number cumulants $\chi_B^{(n)}$ (n=6–10) match lattice at μ_B ≈ 0 and develop non-monotonic trends toward the critical region. [Fu *et al.*, Phys. Rev. D **104**, 094047 (2021)]
- ▶ Real-frequency analysis: two-point flows with analytic continuation resolve σ/π and vector/axial-vector spectral functions and their soft modes at finite T and μ_I . [Wang & Zhuang, Phys. Rev. D 96, 014006 (2017)]

Motivation and Background

- ▶ Understanding the QCD phase diagram at high baryon density is challenging due to the fermion sign problem in lattice QCD.
- ► Effective models (e.g., NJL, QM) provide insight into the chiral phase transition.
- A puzzling feature: FRG studies often show a back-bending of the phase boundary at low temperature an unphysical artifact.
- This behavior may result from pairing instabilities and insufficient regulation in IR.
- Heavy-ion collisions at FAIR/NICA/RHIC produce dense, isospin-asymmetric matter — making this question physically relevant.

Motivation and Background

- A puzzling feature: FRG studies often show a back-bending of the phase boundary at low temperature an unphysical minus entropy.
- ➤ This behavior may result from pairing instabilities and insufficient regulation in IR.

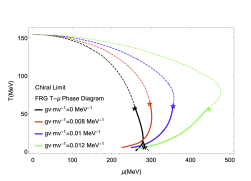


FIG. 2: The phase diagram of the FRG with different vector couplings. Dashed (solid) lines show the second (first) order phase transition. Stars show the tri-critical end point (TGP).

Zhang et al., Phys. Rev. D **96** no. 11 (2017)

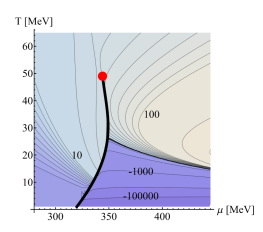


FIG. 4: (color online) The dimensionless entropy density, s_1T^3 is shown as a contour plot together with the CEP and the first-order phase transition line, cf. Fig. [3]. The insect numbers denote the corresponding values of s_1T^3 . Beyond the first-order line, a regime with negative entropy density is found.

Tripolt et al., Phys. Rev. D 97 no. 3 (2018)

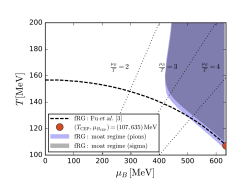


FIG. 1. The phase boundary of the chiral phase transition of QCD [3] together with the moat regime identified though pion and sigma correlations.

W. Fu et al., Phys. Rev. D 111, 094026 (2025).

Table of Contents

Motivation and Background

Chiral Phase Structure with vector mesons

Isospin–Asymmetric QCD at Finite μ_I

Summary

Model Setup

► Two-flavor quark-meson model with scalar σ , pseudoscalar π , vector mesons ω_{μ} , ρ_{μ} .

$$\mathcal{L} = \bar{\psi} \left(i \gamma_{\mu} \partial^{\mu} + \frac{\mu_{I}}{2} \gamma_{0} \tau_{3} + \mu \gamma_{0} \right) \psi
- \bar{\psi} \left[g_{s} \left(\sigma + i \gamma_{5} \boldsymbol{\tau} \cdot \boldsymbol{\pi} \right) + \gamma_{\mu} \left(g_{\omega} \omega^{\mu} + g_{\rho} \boldsymbol{\tau} \cdot \boldsymbol{\rho}^{\mu} \right) \right] \psi
+ \frac{1}{2} \partial_{\mu} \sigma \partial^{\mu} \sigma + \frac{1}{2} \partial_{\mu} \boldsymbol{\pi} \partial^{\mu} \boldsymbol{\pi} - \frac{1}{4} F_{\mu\nu}^{(\omega)} F^{(\omega)\mu\nu} - \frac{1}{4} \boldsymbol{R}_{\mu\nu}^{(\rho)} \boldsymbol{R}^{(\rho)\mu\nu}
- U(\sigma, \boldsymbol{\pi}, \omega_{\mu}, \boldsymbol{\rho}_{\mu}),$$
(1)

- Chemical potentials: μ (quark), μ_I (isospin).
- ▶ Only time components ω_0 , ρ_0^3 are nonzero.

Methods: MF vs FRG

Mean Field Approximation (MF)

▶ Neglects all fluctuations, All mesons treated as mean fields.

Functional Renormalization Group (FRG)

- Non-perturbative; includes quantum and thermal fluctuations.
- Wetterich equation for scale evolution of effective action Γ_k .
- $ightharpoonup \sigma$, π : dynamical; ω_0 , ρ_0^3 : background mean fields.

Flow equation of Effective Potential

$$\partial_{k}U_{k}^{\phi}(T,\mu) = \frac{k^{4}}{12\pi^{2}} \left\{ \frac{3[1 + 2n_{B}(E_{\pi})]}{E_{q}} + \frac{[1 + 2n_{B}(E_{\sigma})]}{E_{\sigma}} - v_{q} \left[\frac{1 - n_{F}(E_{q}, \mu_{\text{eff}}^{+}) - n_{F}(E_{q}, -\mu_{\text{eff}}^{-})}{E_{q}} + \dots \right] \right\}$$
(2)

▶ The effective energies and the masses are given by:

$$E_{\pi} = \sqrt{k^2 + M_{\pi}^2}, \quad E_{\sigma} = \sqrt{k^2 + M_{\sigma}^2}, \quad E_{q} = \sqrt{k^2 + M_{q}^2}$$
(3)
$$M_{q}^2 = g^2 \phi^2, \quad M_{\pi}^2 = 2U_{k}'(\phi^2), \quad M_{\sigma}^2 = 2U_{k}'(\phi^2) + 4\phi^2 U_{k}''(\phi^2)$$
(4)

► The effective quark chemical potentials are:

$$\mu_{\text{eff}}^{\pm} = (\mu - g_{\omega}\omega_{0,k}) \pm (\frac{\mu_I}{2} + g_{\rho}\rho_{0,k}^3)$$
 (5)

Flow equation of ω and ρ

By solving gap equations of U_k :

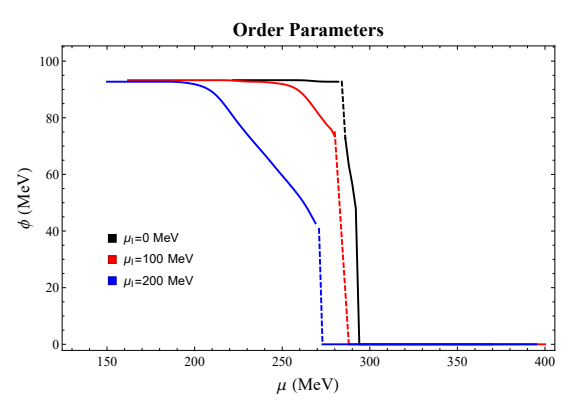
$$\frac{\partial U_k}{\partial \omega_{0,k}} = 0, \qquad \frac{\partial U_k}{\partial \rho_{0,k}^3} = 0.$$
 (6)

The flow equations of ω and ρ become:

$$\partial_{k}\rho_{0,k}^{3} = -\frac{g_{\rho}k^{4}}{\pi^{2}m_{\rho}^{2}E_{q}} \left\{ -\frac{\partial}{\partial\mu_{\text{eff}}^{+}} \left(n_{F}(E_{q},\mu_{\text{eff}}^{+}) + n_{F}(E_{q},-\mu_{\text{eff}}^{+}) \right) + \frac{\partial}{\partial\mu_{\text{eff}}^{-}} \left(\cdots \right) \right\}$$
(7)

$$\partial_{k}\omega_{0,k}^{3} = -\frac{g_{\omega}k^{4}}{\pi^{2}m_{\omega}^{2}E_{q}} \left\{ \frac{\partial}{\partial\mu_{\text{eff}}^{+}} \left(n_{F}(E_{q},\mu_{\text{eff}}^{+}) + n_{F}(E_{q},-\mu_{\text{eff}}^{+}) \right) + \frac{\partial}{\partial\mu_{\text{eff}}^{-}} \left(\cdots \right) \right\}$$
(8)

Chiral condensates: μ_I 's effects

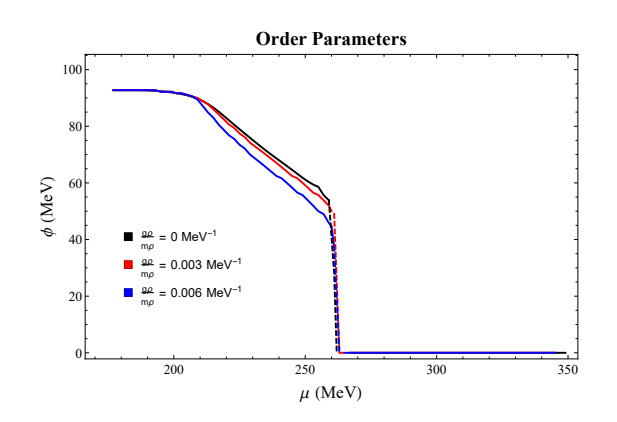


T=10 MeV

Chiral condensates calculated at $g_{\omega}/m_{\omega}=g_{\rho}/m_{\rho}=0.006~[\mathrm{MeV}]^{-1}$. Higher μ_{I} causes the chiral order parameter to collapse at smaller μ and T. This is the expected impact of isospin asymmetry—once μ_{I} approaches m_{π} , pairing in the charged channel destabilizes the chiral minimum.

Son Stephanov, Phys. Rev. Lett. 86 (2001) 592; Kogut Sinclair, Phys. Rev. D 70 (2004) 094501

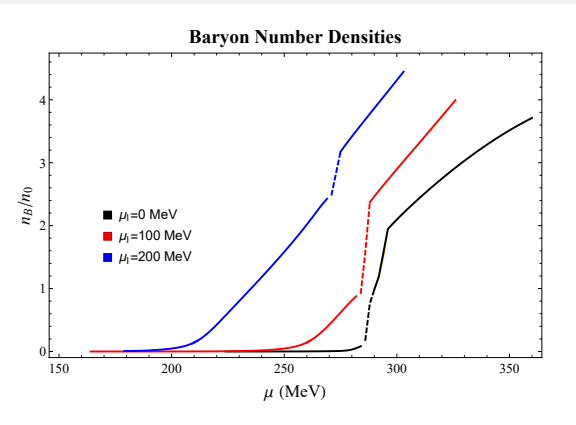
Chiral condensates: vector mesons' effects



Chiral condensates vs. quark chemical potential calculated at T=10 MeV, $\mu_I=200$ MeV, $g_{\omega}/m_{\omega}=0$ [MeV] $^{-1}$.

A repulsive vector interaction shifts the boundary toward larger $\boldsymbol{\mu}$ and weakens the first-order region.

Baryon Number Density

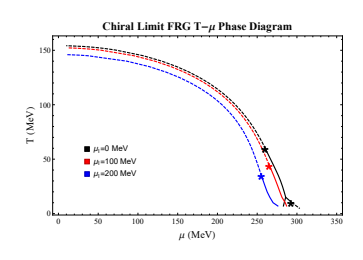


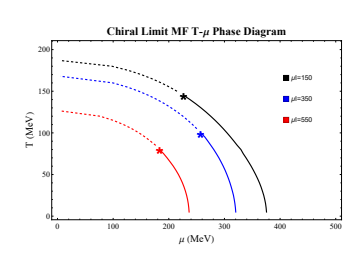
The baryon number density normalized by the nuclear saturation density $n_0 = 0.16 \, \mathrm{fm}^{-3}$ at $T = 10 \, \mathrm{MeV}$ for different μ_I values At low μ_I , a clear first-order phase transition is evident. As μ_I increases, the transition shows a tendency to approach a second-order transition. Additionally, the onset of chiral phase transition shifts to lower quark μ , hinting at the destabilizing influence of isospin asymmetry.

The kink/steepening of $n_{\rm B}(\mu)$ around the boundary is consistent with enhanced baryon-number cumulants in FRG and offers an independent cross-check of the critical

region. Fu Pawlowski, PRD 92 (2015) 116006

Phase Diagram





- ► FRG:
 - Sensitive to isospin chemical potential μ_I and vector meson interactions.
 - ▶ Inclusion of μ_I and ρ meson suppresses back-bending.
 - Tricritical point (TCP) shifts to lower temperature and chemical potential.
 - Shows weaker first-order transitions and smoother crossovers at larger μ_I .
- MF: As μ_I increases, the TCP moves to **lower temperature** and **lower quark chemical potential**.

Mechanism and Physical Insight

Back-bending origin:

- At low T, attractive σ and π exchanges can induce Cooper-like instabilities in dense matter.
- This can lead to unphysical IR behavior in truncated FRG flows.
- Regulator artifacts and truncation (local potential approximation) may amplify this effect.

Suppression mechanisms:

- Finite isospin chemical potential μ_I introduces Fermi surface mismatch between u and d quarks, reducing pairing.
- ρ meson introduces an isospin-dependent repulsive interaction, further stabilizing the system.
- Combined effect shifts the TCP and suppresses the back-bending.

Physical relevance:

- In low-energy heavy-ion collisions, finite μ_I and vector interactions are physically realistic.
- Suppressing back-bending may indicate a more accurate modeling of dense isospin-asymmetric QCD matter.

Table of Contents

Motivation and Background

Chiral Phase Structure with vector mesons

Isospin–Asymmetric QCD at Finite μ_I

Summary

Motivation

- **► Finite isospin density is sign-problem free** ⇒ controllable theory + **lattice access**. Baseline: charged-pion condensation for $\mu_I \gtrsim m_{\pi}$.
- Vector channel matters in data: low-mass dileptons (NA60/CERES) show a strong in-medium ρ broadening rather than a simple mass shift \Rightarrow vector interactions are highly responsive to medium.
- \triangleright ρ in dense matter/EoS: ρ controls the isovector (symmetry) energy in RMF/EFT; a self-consistent isovector response $\langle \rho_0^3 \rangle$ links QCD phase structure to neutron-rich matter.
- **Therefore:** study isovector mismatch (μ_I) + isovector repulsion (g_{ρ}) as two stabilizers of the low-T FRG flow and of the phase-boundary topology.

Key references

(1) Son & Stephanov, Phys. Rev. Lett. 86 (4) NA60 Coll., Eur. Phys. J. C 61 (2009) (2001) 592. 711–720:

(2) Kogut & Sinclair, *Phys. Rev. D* **66** *Phys. Rev. Lett.* **100** (2008) 022302. (2002) 034505. (5) Drews & Weise, *Prog. Part. Nucl.* _{20/32} 2002) 034505.

U E DI I C 11 DI 02 (0017) CO 107

Tests with $\mu_I \& \rho$

- **Back-bending suppression:** low-T phase boundary becomes monotonic once mismatch + repulsion flatten multi-minima in U_{k} .
- ▶ **CEP/TCP drift:** T_{TCP} moves *down*; boundary in T- μ shifts to *larger* μ when g_{ρ} increases, but to *smaller* μ as μ_{I} grows.
- ▶ ρ -response region: 2nd-order onset at small μ_I , turning into a 1st-order boundary at larger μ_I/μ .
- ▶ **Nonmonotonic** $\langle \rho_0^3 \rangle (\mu)$ **at fixed** μ_l **:** rises then falls across chiral restoration as flavor densities rebalance.
- ▶ Consistency checks: vector-sensitive observables (dileptons), lattice at finite μ_I , and dense-matter constraints on symmetry energy.

Flow equation of Effective Potential

In the previous flow equations, only the ρ meson was retained, with $g_{\omega}=0$.

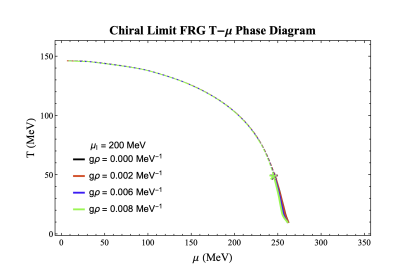
$$\partial_{k}U_{k}^{\phi}(T,\mu) = \frac{k^{4}}{12\pi^{2}} \left\{ \frac{3[1 + 2n_{B}(E_{\pi})]}{E_{q}} + \frac{[1 + 2n_{B}(E_{\sigma})]}{E_{\sigma}} - v_{q} \left[\frac{1 - n_{F}(E_{q}, \mu_{eff}^{+}) - n_{F}(E_{q}, -\mu_{eff}^{-})}{E_{q}} + \dots \right] \right\}$$

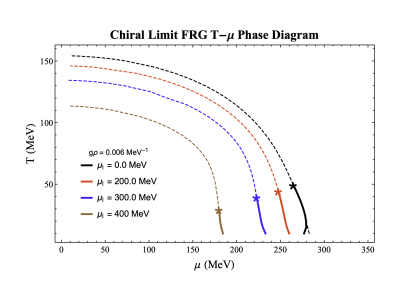
$$\partial_{k}\rho_{0,k}^{3} = -\frac{g_{\rho}k^{4}}{\pi^{2}m_{\rho}^{2}E_{q}} \left\{ -\frac{\partial}{\partial\mu_{eff}^{+}} \left(n_{F}(E_{q}, \mu_{eff}^{+}) + n_{F}(E_{q}, -\mu_{eff}^{+}) \right) + \dots \right\}$$

$$\mu_{eff}^{\pm} = \mu \pm \left(\frac{\mu_{I}}{2} + g_{\rho}\rho_{0,k}^{3} \right)$$

$$(10)$$

Chiral-limit $T-\mu$ phase diagram

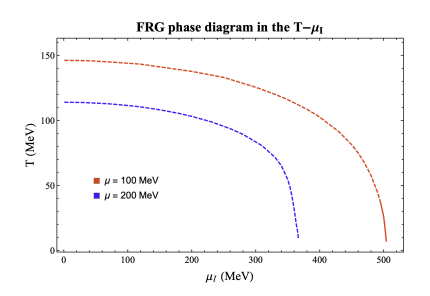




- ▶ Left panel (fixed $\mu_I = 200$ MeV): Increasing g_ρ pushes the chiral boundary to larger μ , lowers $T_{\rm TCP}$, and shrinks the low-T first-order wedge.
- ▶ Right panel (fixed $g_{\rho}/m_{\rho}=0.006$ MeV⁻¹): Larger μ_{I} moves the boundary left/down (earlier restoration), again reducing $T_{\rm TCP}$.

Tripolt et al., Phys. Rev. D 97 (2018) 034022.

T– μ_I phase diagrams at fixed μ

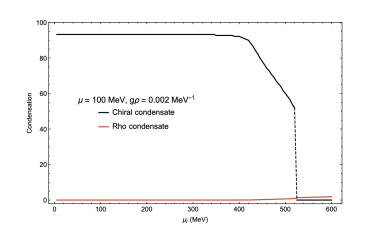


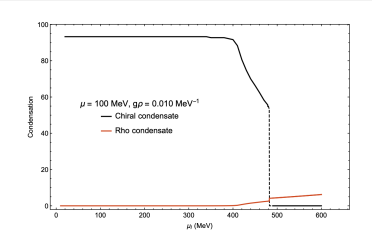
- ► FRG with self-consistent ρ_0^3 yields a distinct **isovector region** $(\rho_0^3 \neq 0)$. The **onset** of ρ_0^3 is **continuous (2nd order)** at lower μ_I ; a **1st-order boundary** appears at larger μ_I/μ where the chiral minimum jumps.
- ▶ **Increasing** μ reshapes both lines: μ_I^{crit} shifts and the length of the 1st-order segment changes, reflecting the density dependence of the chiral–isovector coupling.

The left shift of the chiral boundary with larger μ_I matches analytic and lattice expectations.

Brauner & Huang, Phys. Rev. D 94 (2016) 094003.

Chiral vs ρ condensates

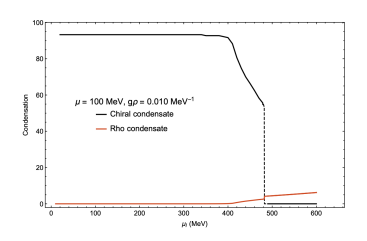


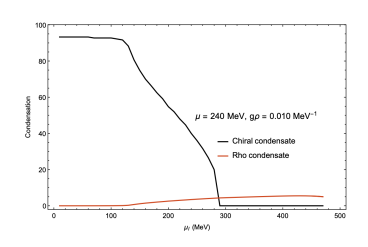


- **Setup:** T=10 MeV, $\mu=100$ MeV; $g_{\rho}/m_{\rho}=0.002,\,0.010$ MeV $^{-1}$.
- $ho \langle \rho_0^3 \rangle$ shows a **continuous onset** near μ_I^{crit} , followed at μ_I^{crit} by a **discontinuous rearrangement** synchronized with a drop of φ (mixed 1st order).
- Stronger g_{ρ} shifts both thresholds and reduces multi-minima competition in U_k (repulsive stabilization of the low-T flow).

Near chiral restoration, vector/axial-vector modes broaden and nearly degenerate. The ρ channel competes with the chiral condensate and reshapes U_k , explaining the mutual "pull" seen in the curves—this is a coupled dynamical interplay rather than two

Chiral vs ρ condensates

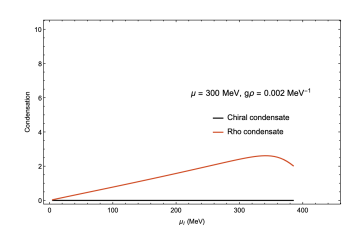


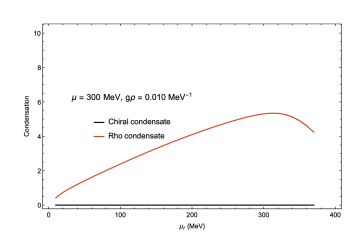


- ▶ **Setup:** T = 10 MeV, $\mu = 200$ MeV; same g_{ρ}/m_{ρ} scan.
- ▶ Both the 2nd-order **onset** and the **1st-order** rearrangement move to different μ_I than at $\mu=100$ MeV, reflecting a stronger density background.
- ▶ A plateau/shoulder in $\langle \rho_0^3 \rangle (\mu_I)$ with a synchronized drop of $\varphi(\mu_I)$ reproduces the 2nd \rightarrow 1st sequence visible on the maps.

Tripolt et al., Phys. Rev. D 89 (2014) 034010.

Chiral vs ρ condensates

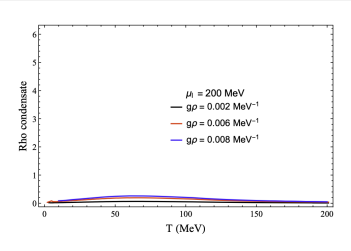


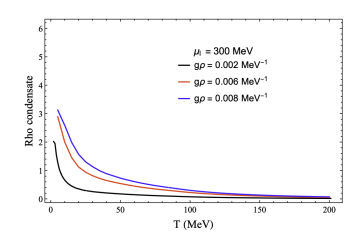


- **Setup:** T = 10 MeV, $\mu = 300$ MeV; compare $g_{\rho}/m_{\rho} = 0.002$ and 0.010 MeV⁻¹.
- Larger g_{ρ} enhances isovector repulsion, making the ρ condensate dominate the order-parameter dynamics, while the chiral condensate is almost completely quenched. The system becomes increasingly controlled by the vector channel at strong coupling, reinforcing the view that isovector repulsion reshapes the low-T phase structure.

Tripolt et al., Phys. Rev. D 97 (2018) 034022.

Thermal evolution of ρ condensates





28 / 32

- **Coupling dependence:** Larger g_{ρ} enhances the magnitude of ρ condensates but does not change their qualitative T dependence.
- **Physical interpretation:** Finite temperature tends to **melt** the isovector order, while stronger repulsion strengthens it at low T. This interplay explains why ρ effects are most relevant for cold, dense matter.

Raising T softens the ρ mode and drives ρ – a_1 degeneracy. The decrease of the condensate follows the chiral trend and signals proximity to (partial) restoration. Jung von Smekal, Phys. Rev. D 95 (2017) 036020

Phase diagram in $\omega - \mu_I$

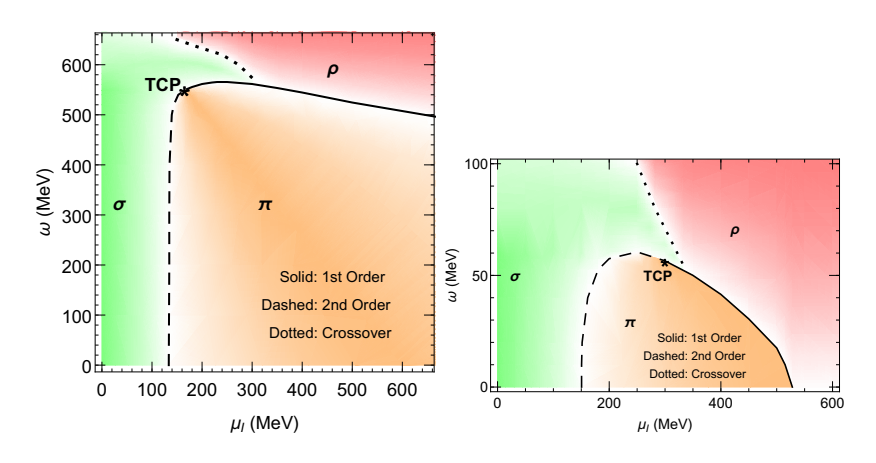


Figure: (left) $\mu = 0$, (right) $\mu = 250 MeV$

New phase diagram, New Tri-Critical End Point!

Zhang, Hou, Liao, Chin. Phys. C 44 (2020) 11, 111001s

Table of Contents

Motivation and Background

Chiral Phase Structure with vector mesons

Isospin–Asymmetric QCD at Finite μ_{I}

Summary

Summary

- Finite μ_I + isovector repulsion (g_ρ) reshape the low-T landscape: **earlier** chiral restoration, **smaller** first-order wedge, **lower** $T_{\rm TCP}$.
- ► The ρ -condensate region has a **2nd-order onset** and a **1st-order boundary** at larger μ_I/μ .
- ▶ Back-bending is suppressed by the combined effect of Fermi-surface mismatch and repulsion.

Happy birth day to Prof. Jan M. Pawlowski